7th ECCOMAS Thematic Conference on Smart Structures and Materials
SMART 2015
A.L. Araújo, C.A. Mota Soares, et al. (Editors)

PHENOMENOLOGICAL AND PHYSICALLY MOTIVATED CONSTITUTIVE MODELS FOR FERROMAGNETIC AND MAGNETOSTRICTIVE MATERIALS

Artjom Avakian[*] and Andreas Ricoeur[†]

[*, †] Institute of Mechanics, University of Kassel, Mönchebergstr. 7, 34125 Kassel, Germany

[*]artjom.avakian@uni-kassel.de

[†]andreas.ricoeur@uni-kassel.de

Key words: Ferromagnetics, magnetostriction, hysteresis loops, nonlinear constitutive modeling, Barkhausen jumps, domain wall motion.

Summary: *The coupling of magnetic and mechanical fields due to the constitutive behavior of a material is commonly denoted as magnetostrictive effect. The latter is only observed with large coupling coefficients in ferromagnetic materials, where coupling is caused by the rotation of the domains as a result of magnetic (Joule effect) or mechanical (Villari effect) loads. However, only a few elements (e.g. Fe, Ni, Co, Mn) and their compositions exhibit such a behavior.*

In this paper, the theoretical background of nonlinear constitutive multifield behavior as well as the Finite Element (FE) implementation are presented. Nonlinear material models describing the ferromagnetic behavior are presented. Both physically and phenomenologically motivated constitutive models have been developed for the numerical calculation of the nonlinear magnetostrictive behaviors. On this basis, magnetization strain and stress are simulated and the resulting effects analyzed. The phenomenological approach covers reversible nonlinear behavior as it is observed e.g. in cobalt ferrite. Numerical simulations based on the physically motivated model focus on the calculation of hysteresis loops and the prediction of local domain orientations and residual stress going along with the magnetization process.

1 INTRODUCTION AND MOTIVATION

Ferromagnetic behavior has been well known and technically exploited for centuries. Although there are still plenty of research activities in the physics community, the principles of ferromagnetism are well understood nowadays. For engineering applications, the knowledge of the macroscopic material behavior is in most applications more essential than a deep understanding of the physics on the atomic scale. Magnetostriction is technically exploited in actuation systems and there are a variety of applications for permanent magnetic fields in poled ferromagnetic devices. New concepts combine ferromagnetic and ferroelectric phases in so-called multiferroic composites [1]-[6] in order to induce a coupling of electric and magnetic fields.

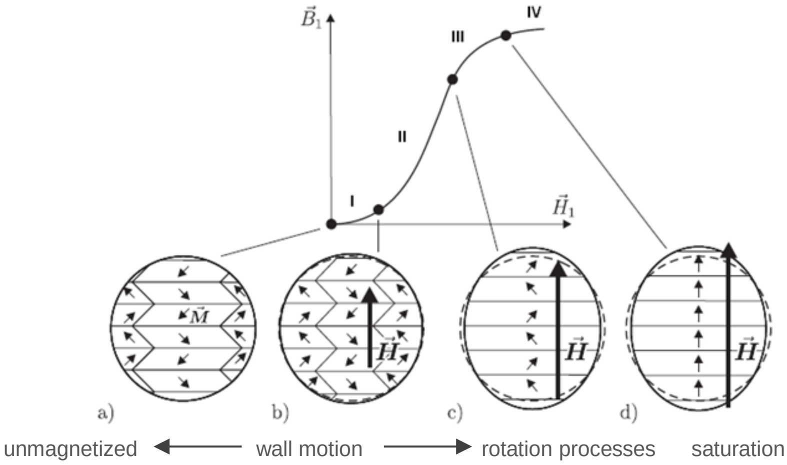

Fig. 1: Initial magnetization curve [7]

All these applications require the knowledge of the constitutive behavior of the employed ferromagnetic material. Therefore, plots of the magnetic induction vs. the magnetic field are mostly provided by manufacturing companies. The same holds for the strain vs. magnetic field, if the material is suitable for magnetostrictive application. On the other hand, stress vs. strain characteristics are equally important, however scarcely available. Some ferromagnetic materials exhibit a pronounced hysteresis behavior, others show an almost reversible nonlinear characteristic. Even two specimens with an identical chemical composition can exhibit different features, depending e.g. on the sintering conditions. The reason for the different behaviors is found on the micro scale of domain or Bloch walls as depicted in Fig. 1 for a typical plot of magnetic induction vs. magnetic field [8]-[13].

In Fig. 2, ferromagnetic hysteresis loops in terms of magnetization and magnetostriction vs. magnetic field are shown on the left hand side. In the experiments, specimens of Galfenol have been exposed to combined magnetomechanical loading imposing a compressive stress. In Fig. 3, magnetization and engineering strain are plotted vs. the magnetic field, now for cobalt ferrite. In contrast to Fig. 2, there is almost no hysteresis behavior, in fact the material shows nearly reversible characteristics. On the other hand, cobalt ferrite is also known with pronounced hysteresis behaveor, if exposed to different manufacturing procedures [14].

From the modeling point of view, it is crucial to develop a mathematical framework describing the constitutive behavior of ferromagnetic materials as accurate as possible. Here, both features of reversible and irreversible characteristics have to be covered by different modeling approaches. In connection with a finite element implementation based on the weak formulation of balance laws, a valuable numerical tool is available to predict the multifield-behavior of so-called smart devices and to improve their performance e.g. the magnetoelectric coupling in a multiferroic composite.

In this paper, two approaches are presented for the constitutive modeling of ferromagnetic materials. The one is akin to a model for ferroelectrics and is based on microphysical considerations [15], [16]. It takes advantage of the fact that ferromagnetic and ferroelectric effects, although originating from completely different processes on the atomic scale, show comparable features on the micro and meso levels. In Fig. 2, ferromagnetic and ferroelectric hystereses are compared. Similarities are obvious as well as differences. The ferromagnetic curves exhibit a saturation for larger loads and the remanent quantities are smaller. The other ap-

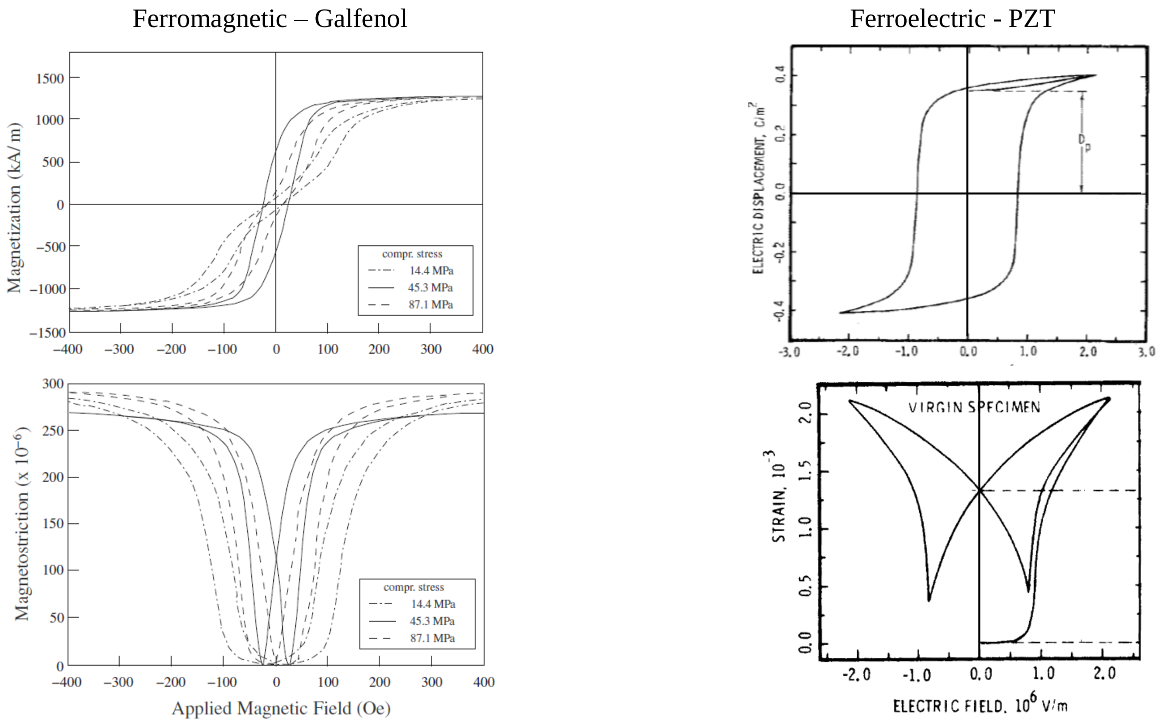

Fig. 2: Hysteresis loops, left: ferromagnetic [17], right: ferroelectric [18]

proach is purely phenomenological starting from a thermodynamical potential and providing a reversible nonlinear behavior. Both models have been implemented into a finite element software to solve complex boundary value problems. In this paper, however, the focus is on the constitutive behavior, demonstrated at simple bulk specimens under uni- or multiaxial magnetomechanical loadings.

2 CONSTITUTIVE BEHAVIOR: COMPARISON OF MODELS

Before explaining the modeling approaches more detailed, the constitutive frameworks of ferroelectric and ferromagnetic as well as reversible and irreversible behaviors are summarized and compared to each other. Ferroelectric behavior is commonly governed by the fol-

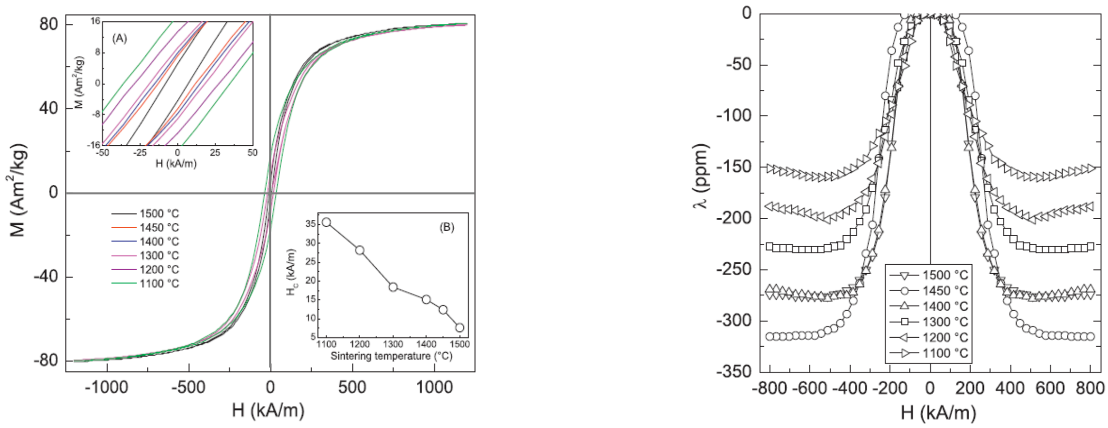

Fig. 3: Magnetization and magnetostriction curves of cobalt ferrite at room temperature for samples sintered at different temperatures as a function of magnetic field [14]

lowing equations [15]:

$$\begin{aligned} \sigma_{ij} &= c_{ijkl}\left(\varepsilon_{kl} - \varepsilon_{kl}^{irr}\right) - e_{lij}E_l\,, \\ D_l &= e_{lij}\left(\varepsilon_{ij} - \varepsilon_{ij}^{irr}\right) + \kappa_{ln}E_n + P_l^{irr}, \\ B_k &= \mu_{km}H_m\,. \end{aligned} \tag{1}$$

The irreversible strain ε_{kl}^{irr} and polarization P_l^{irr} are described within a microphysical framework, accounting for domain wall motion. Considering plane problems, the latter is controlled by four internal variables and an evolution equation satisfying the Clausius-Duhem inequality. Due to intended applications within a multi-physics framework, the ferroelectric material is allocated a magnetic permeability expressed by the third equation. The material tensors also depend on the internal variables, giving rise to another source of nonlinearity, even in the magnetic permittivity. The piezoelectric coefficients e.g. relate stresses σ_{ij} and the electric field E_l.

Based on the same ideas as Eq. (1), the ferromagnetic constitutive equations read

$$\begin{aligned} \sigma_{ij} &= c_{ijkl}\left(\varepsilon_{kl} - \varepsilon_{kl}^{irr}\right), \\ D_l &= \kappa_{ln}E_n\,, \\ B_k &= \mu_{km}H_m + M_k^{irr}. \end{aligned} \tag{2}$$

Here, irreversible strain and magnetization are likewise governed by four internal variables describing Bloch wall motion due to magnetoelectric energies. In contrast to ferroelectricity, a piezomagnetic coefficient relating magnetic field and stress or strain and magnetic induction is not involved, accounting for the saturation depicted in Fig. 2. As a second consequence, the irreversible strain does not directly induce a magnetic induction B_k. Dielectric properties are allocated by the second equation which is linear only at the first glance, since the dielectric constants κ_{ln} are controlled by the internal variables in a nonlinear manner.

The constitutive equations of nonlinear reversible ferromagnetic behavior are finally given by

$$\begin{aligned} \dot{\sigma}_{ij} &= c_{ijkl}(\varepsilon, H)\dot{\varepsilon}_{kl} - q_{kij}(\varepsilon, H)\dot{H}_k\,, \\ \dot{D}_l &= \kappa_{ln}(E)\dot{E}_n\,, \\ \dot{B}_k &= q_{kij}(\varepsilon, H)\dot{\varepsilon}_{ij} + \mu_{km}(\varepsilon, H)\dot{H}_m\,, \end{aligned} \tag{3}$$

where a rate dependent depiction has been chosen. The nonlinearity is completely included in the dependence of the material coefficients on the independent variables. Due to the reversibility of the constitutive behavior, these functions are unique.

3 CONSTITUTIVE MODELS OF FERROMAGNETIC MATERIALS

3.1 Physically motivated ferromagnetic model

The physically based nonlinear constitutive relations of a ferromagnetic material with dielectric properties are based on a suitable thermodynamic potential $\Psi\ (\varepsilon_{ij}, E_l, H_k)$ with strain, electric and magnetic fields as independent variables:

$$\Psi\left(\varepsilon_{ij}, E_l, H_k\right) = \frac{1}{2} c_{ijkl}\varepsilon_{kl}\varepsilon_{ij} - \frac{1}{2}\kappa_{ln} E_l E_n - \frac{1}{2}\mu_{km} H_k H_m - c_{ijkl}\varepsilon_{kl}^{irr}\varepsilon_{ij} - M_k^{irr} H_k \,. \tag{4}$$

Here, ε_{ij} denotes the strain within a theory on infinitely small deformations. Eq. (4) is based on the common assumption, that the strain ε_{ij} and magnetic induction B_k are additively decomposed into reversible and irreversible parts:

$$\varepsilon_{ij} = \varepsilon_{ij}^{r} + \varepsilon_{ij}^{irr}, \qquad B_k = B_k^{r} + M_k^{irr}. \tag{5}$$

The irreversible parts are due to Barkhausen jumps on the microlevel or domain wall motion on the mesoscopic level, see Fig. 1. Reversible quantities will from now on be denoted with the superscript "r" and irreversible quantities with "irr". Concerning the electric displacement, weak nonlinearities are assumed due to changes of the dielectric constants as a consequence of Bloch wall motion, thus $D_l = D_l^r$.

The constitutive equations of nonlinear ferromagnetic behavior are then given by

$$\begin{aligned}
\sigma_{ij} &= \left.\frac{\partial\Psi(\varepsilon_{ij}, E_l, H_k)}{\partial\varepsilon_{ij}}\right|_{E_l, H_k} = c_{ijkl}\left(\varepsilon_{kl} - \varepsilon_{kl}^{irr}\right), \\
D_l &= -\left.\frac{\partial\Psi\left(\varepsilon_{ij}, E_l, H_k\right)}{\partial E_l}\right|_{\varepsilon_{ij}, H_k} = \kappa_{ln} E_n \,, \\
B_k &= -\left.\frac{\partial\Psi\left(\varepsilon_{ij}, E_l, H_k\right)}{\partial H_k}\right|_{\varepsilon_{ij}, E_l} = \mu_{km} H_m + M_k^{irr} \,.
\end{aligned} \tag{6}$$

The irreversible strain ε_{ij}^{irr} and magnetization M_k^{irr} are due to domain wall motion. On the continuum level they are described by internal variables ν_n, for plane problems associated with the four possible orientations of domains in a grain, with the “easy axis“ in the $\langle 100\rangle$ direction (see Fig. 4) [10]-[13]:

$$\dot{\varepsilon}_{ij}^{irr} = \sum_{n=1}^{4} \overset{(n)}{\varepsilon}{}_{ij}^{sp}\dot{\nu}_n \,, \qquad \dot{M}_k^{irr} = \sum_{n=1}^{4} \Delta\overset{(n)}{M}{}_k^{sp}\dot{\nu}_n \,, \tag{7}$$

where $\overset{(n)}{\varepsilon}{}_{ij}^{sp}$ and $\Delta\overset{(n)}{M}{}_k^{sp}$ represent the spontaneous strain and change of spontaneous magnetization for the domain n, respectively. In all calculations, the generalized state of plane stress will be assumed, i.e. $\sigma_{i3} = 0, D_3 = 0, B_3 = 0$. The changes of magnetization exhibit three possibilities, $\pm 90°$ and $180°$, for each domain species $n = 1, \ldots, 4$. In Fig. 4, one variant for $n = 3$ is depicted as an example, i.e. $\Delta\overset{(3)}{M}{}_k^{sp} = \overset{(4)}{M}{}_k^{sp} - \overset{(3)}{M}{}_k^{sp}$ for $+90°$ jumping. Concerning the spontaneous strains, each domain species ν is allocated one unique tensor representing $\pm 90°$ jumping.

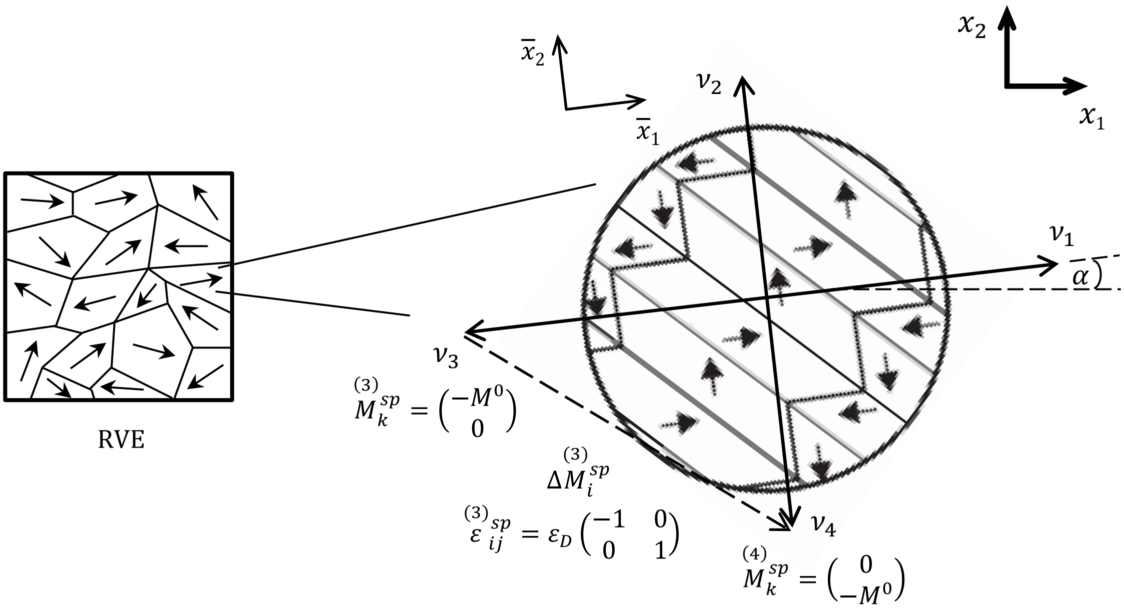

Fig. 4: Internal variables ν_n and the magnetic orientations in a grain with local coordinate system $(\bar{x}_1, \bar{x}_2)$. Characterization of the orientation of domain variants $n = 1, \ldots, 4$ with respect to the global coordinate system (x_1, x_2) by an angle α

The total change of volumes of the domain species in a grain resulting from Bloch wall motion is conserved by the following relations

$$0 \leq \nu_n \leq 1 \,, \qquad \sum_{n=1}^{4} \nu_n = 1 \;, \tag{8}$$

where ν_n stands for the specific volume of each domain. The rates of volume change of the species $\dot{\nu}_n$, i.e. the time derivatives of the internal variables, play an important role in the thermodynamical formulation of the material law. The evolution of the internal variables ν_n within a domain structure is controlled by an energetic criterion, which has been chosen in the style of ferroelectric switching criteria [19], [20]:

$$\Delta w^n = \sigma_{ij} \overset{(n)}{\varepsilon}{}_{ij}^{sp} + \Delta \overset{(n)}{M}{}_k^{sp} H_k \geq w^{crit} \,. \tag{9}$$

The left hand side of the inequality, consisting of mechanical and magnetic contributions, represents the dissipative work Δw^n of Bloch wall motion due to the jumping of a species n.

On the microlevel, Barkhausen jumping occurs when the dissipative energy exceeds an associated critical value w^{crit}. In-plane, there are three possible jumping variants with the “easy axis“ in the $\langle 100 \rangle$ direction, going along with two different threshold values being identical to those of ferroelectric switching [19], [21]:

$$w^{crit} = \begin{cases} \sqrt{2} M^0 H_c & \pm 90^\circ \\ 2 M^0 H_c & 180^\circ \end{cases} , \tag{10}$$

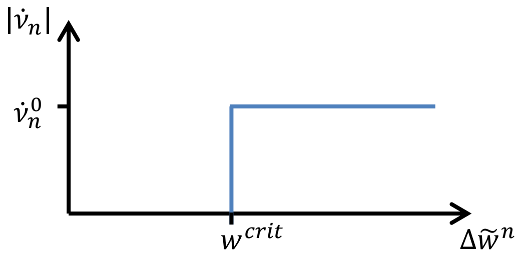

Fig. 5: Evolution law for internal variables ν_n

where the material parameters H_c and M^0 are the coercive field and the magnitude of spontaneous magnetization. Obviously, the left hand side of the inequality (9) is always positive if Barkhausen jumps occur, satisfying the Clausius-Duhem inequality and thus guarantying the thermodynamical consistency of the evolution law.

On the macroscopic level, an evolution law for the internal variables ν_n controls Bloch wall motion. Based on Eq. (9) the evolution law for a jumping species n is

$$\dot{\nu}_n = -\dot{\nu}_n^0\,\mathcal{H}\left(\frac{\Delta\widetilde{w}^n}{w^{crit}} - 1\right), \qquad \Delta\widetilde{w}^n = \max\left(\Delta w^n_{\pm 90°}, \Delta w^n_{180°}\right). \tag{11}$$

Here, $\mathcal{H}(..)$ is the Heaviside-function (see Fig. 5) and $\dot{\nu}_n^0$ is a model parameter. The latter represents a discrete amount of domain wall motion, which has to be chosen within a numerical context. Eq. (11) determines, if the volume of the species n decreases due to jumping or not. The reduction of ν_n always occurs in favour of another species, see Eq. (8).

While the changes of strain and spontaneous magnetization due to Bloch wall motion are controlled by Eq. (7), the evolution of material tangents in an RVE or grain is likewise connected to the internal variables:

$$c_{ijkl} = \sum_{n=1}^{4} \overset{(n)}{c}_{ijkl}\,\nu_n \quad \rightarrow \quad \dot{c}_{ijkl} = \sum_{n=1}^{4} \overset{(n)}{c}_{ijkl}\,\dot{\nu}_n = \sum_{n=1}^{4} \frac{\partial c_{ijkl}}{\partial \nu_n}\dot{\nu}_n \tag{12}$$

and similar

$$\kappa_{ln} = \sum_{n=1}^{4} \overset{(n)}{\kappa}_{ln}\,\nu_n\,, \qquad \mu_{km} = \sum_{n=1}^{4} \overset{(n)}{\mu}_{km}\,\nu_n\,. \tag{13}$$

3.2 Phenomenologically motivated ferromagnetic model

The constitutive behavior is assumed to be governed by the thermodynamic potential

$$\begin{aligned}\bar{\Psi}\left(\sigma_{ij}, E_l, H_k\right) = &-\frac{1}{2}S_{11}\sigma_1\sigma_1 - S_{12}\sigma_1\sigma_2 - S_{13}\sigma_1\sigma_3 - \frac{1}{2}\kappa_{11}E_1E_1 - \frac{1}{2}\bar{\mu}^0_{11}H_1H_1 \\ &- \frac{\eta_1}{1+\zeta_1 H_1^{-3}}\sigma_1 - \frac{\eta_2}{1+\zeta_2 H_1^{-3}}\sigma_2 - \rho\{H_1 - \xi\, ln(\xi + H_1)\}\,,\end{aligned} \tag{14}$$

where stress, electric and magnetic fields are preliminarily chosen as independent variables. Within the context of a simple model, the coefficients η_i, ζ_i, ρ and ξ are adapted to experimental curves. Eq. (14) has been formulated in a principal stress state, thus shear stress does not appear in the potential. The constitutive behavior is obtained by differentiation of Eq. (14) according to

$$\begin{aligned} d\varepsilon_{ij}(d\sigma_{kl}, dE_l, dH_k) &= \frac{-\partial^2\overline{\Psi}}{\partial\sigma_{ij}\partial\sigma_{kl}}d\sigma_{kl} + \frac{-\partial^2\overline{\Psi}}{\partial\sigma_{ij}\partial E_l}dE_l + \frac{-\partial^2\overline{\Psi}}{\partial\sigma_{ij}\partial H_k}dH_k\,, \\ dE_l\big(d\sigma_{ij}, dE_n, dH_k\big) &= \frac{-\partial^2\overline{\Psi}}{\partial E_l\partial\sigma_{kl}}d\sigma_{ij} + \frac{-\partial^2\overline{\Psi}}{\partial E_l\partial E_n}dE_n + \frac{-\partial^2\overline{\Psi}}{\partial E_l\partial H_k}dH_k\,, \\ dB_k\big(d\sigma_{ij}, dE_l, dH_m\big) &= \frac{-\partial^2\overline{\Psi}}{\partial H_k\partial\sigma_{ij}}d\sigma_{ij} + \frac{-\partial^2\overline{\Psi}}{\partial H_k\partial E_l}dE_l + \frac{-\partial^2\overline{\Psi}}{\partial H_k\partial H_m}dH_m\,, \end{aligned} \tag{15}$$

where the material coefficients, e.g. S_{11}, S_{12}, are assumed to be constant within incremental changes of state and thus the rate dependent constitutive framework is given by

$$\begin{aligned} \dot{\varepsilon}_{ij}\big(\dot{\sigma}_{kl}, \dot{E}_l, \dot{H}_k\big) &= s_{ijkl}\dot{\sigma}_{kl} - Q_{kij}\dot{H}_k\,, \\ \dot{D}_l\big(\dot{\sigma}_{ij}, \dot{E}_n, \dot{H}_k\big) &= \kappa_{ln}\dot{E}_n\,, \\ \dot{B}_k\big(\dot{\sigma}_{ij}, \dot{E}_l, \dot{H}_m\big) &= Q_{kij}\dot{\sigma}_{ij} + \bar{\mu}_{km}\dot{H}_m\,. \end{aligned} \tag{16}$$

Eqs. (16) represent nonlinear but, in contrast to the microphysical model, reversible changes of state. The electric displacement just depends on the electric field, in a ferromagnetic material not being coupled with mechanical or magnetic fields. Eq. (16) representing multi-axial loading states in terms of tensorial representation, the responses e.g. in the x_1-direction are obtained as

$$d\varepsilon_1\big(d\sigma_q, dE_i, dH_i\big) = S_{11}d\sigma_1 + S_{12}d\sigma_2 + S_{13}d\sigma_3 + 3\frac{\eta_1\zeta_1H_1^2}{(\zeta_1+H_1^3)^2}dH_1\,, \tag{17}$$

$$dD_1\big(d\sigma_q, dE_i, dH_i\big) = \kappa_{11}dE_1\,, \tag{18}$$

$$\begin{aligned} dB_1\big(d\sigma_q, dE_i, dH_i\big) = {} & 3\frac{\eta_1\zeta_1H_1^2}{(\zeta_1+H_1^3)^2}d\sigma_1 + 3\frac{\eta_2\zeta_2H_1^2}{(\zeta_2+H_1^3)^2}d\sigma_2 + \Bigg(\bar{\mu}_{11}^0 \\ & + \frac{6\eta_1\zeta_1H_1(\zeta_1-2H_1^3)\sigma_1}{(\zeta_1+H_1^3)^3} + \frac{6\eta_2\zeta_2H_1(\zeta_2-2H_1^3)\sigma_2}{(\zeta_2+H_1^3)^3} + \frac{\rho\xi}{(\xi+H_1)^2}\Bigg)dH_1\,. \end{aligned} \tag{19}$$

In general, all material coefficients depend on the three independent variables. Experimental observations, however, put this thermodynamical requirement into perspective, showing e.g. a noticeable nonlinearity of the stress-strain curve only for highly magnetostrictive materials. The simple potential according to Eq. (14) is setting the magnetostrictive constants as a function of just the magnetic field and the magnetic permittivity as a function of both magnetic field and stress:

$$Q_{111} = 3\frac{\eta_1\zeta_1H_1^2}{(\zeta_1+H_1^3)^2}\,, \qquad Q_{122} = 3\frac{\eta_2\zeta_2H_1^2}{(\zeta_2+H_1^3)^2} \tag{20}$$

$$\bar{\mu}_{11} = \bar{\mu}_{11}^{0} + \frac{6\eta_1\zeta_1 H_1(\zeta_1 - 2H_1^3)\sigma_1}{(\zeta_1 + H_1^3)^3} + \frac{6\eta_2\zeta_2 H_1(\zeta_2 - 2H_1^3)\sigma_2}{(\zeta_2 + H_1^3)^3} + \frac{\rho\xi}{(\xi + H_1)^2}\,. \tag{21}$$

A more sophisticated model replaces the constant coefficients ζ_1, ζ_2 and ξ by variables depending on the stresses:

$$\begin{gathered} \zeta_1 = \zeta_1^0 + \zeta_1^\sigma(\sigma_1 - \sigma_2)\,, \qquad \zeta_2 = \zeta_2^0 + \zeta_2^\sigma(\sigma_1 - \sigma_2) \\ \xi = \xi^0 + \xi^\sigma(\sigma_1 - \sigma_2)\,. \end{gathered} \tag{22}$$

Both variants of the phenomenological constitutive model will be investigated in the next section. For the numerical implementation, the independent mechanical variable is changed from stress to strain. Accordingly, the material tensors are subject to the following transformations:

$$c_{ijkl} = s_{ijkl}^{-1}\,, \qquad q_{kij} = Q_{kln}c_{lnij}\,, \qquad \mu_{km} = \bar{\mu}_{km} - Q_{kln}c_{lnij}Q_{mij}\,. \tag{23}$$

The constitutive equations for the nonlinear reversible ferromagnetic behavior are thus given as

$$\begin{aligned} \dot{\sigma}_{ij}\big(\dot{\varepsilon}_{kl}, \dot{E}_l, \dot{H}_k\big) &= c_{ijkl}\dot{\varepsilon}_{kl} - q_{kij}\dot{H}_k\,, \\ \dot{D}_l\big(\dot{\varepsilon}_{ij}, \dot{E}_n, \dot{H}_k\big) &= \kappa_{ln}\dot{E}_n\,, \\ \dot{B}_k\big(\dot{\varepsilon}_{ij}, \dot{E}_l, \dot{H}_m\big) &= q_{kij}\dot{\varepsilon}_{ij} + \mu_{km}\dot{H}_m\,. \end{aligned} \tag{24}$$

4 Results

The two constitutive models according to Sec. 3 have been implemented within the framework of the finite element method, starting from a weak formulation of the balance equations of electro-, magneto- and elastostatics:

$$\sigma_{ij,j} = 0, \qquad D_{l,l} = 0, \qquad B_{k,k} = 0\,. \tag{25}$$

The material parameters of cobalt ferrite, which has been chosen for the sake of demonstration, are presented in [22]. Moreover, the following quantities have been used for the physically motivated model:

$H_c = 626$ Oe [23], $M^0 = 150\ \mathrm{Am^2kg^{-1}}$ and $\varepsilon_D = 0.03$.

For the phenomenological model, the following coefficients are used:

$\eta_1 = -131e-6,\ \eta_2 = 106e-6,\ \zeta_1^0 = 5.5e+15\ \mathrm{A^3m^{-3}},\ \zeta_2^0 = 2.1e+15\ \mathrm{A^3m^{-3}},\ \zeta_1^\sigma = 3e+9\ \mathrm{A^3N^{-1}m^{-1}},\ \zeta_2^\sigma = 1{,}145e+9\ \mathrm{A^3N^{-1}m^{-1}},\ \rho = 0.6\ \mathrm{T},\ \xi^0 = 1e+5\ \mathrm{NV^{-1}s^{-1}},\ \xi^\sigma = 1e-2\ \mathrm{m^2V^{-1}s^{-1}}$.

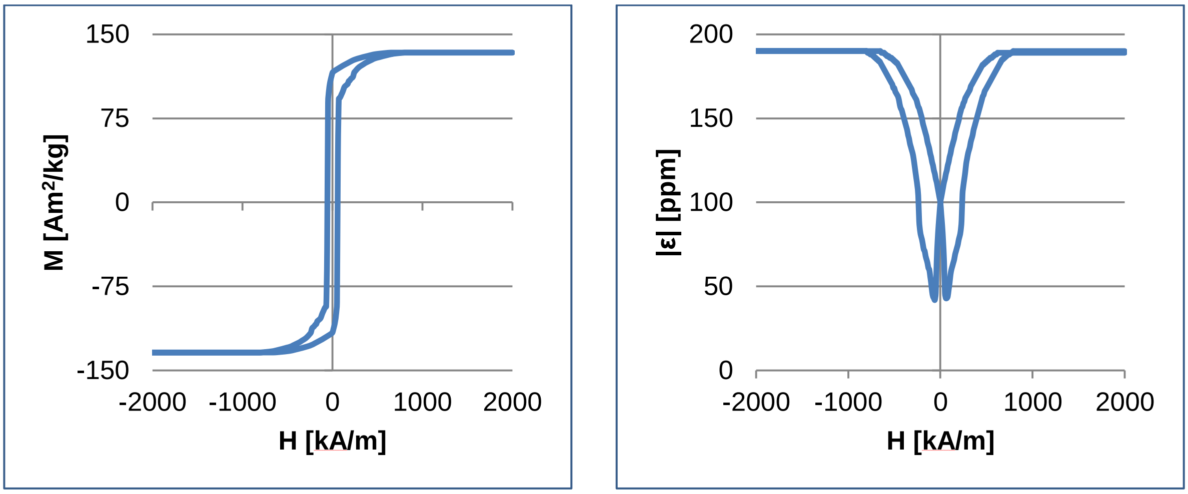

Fig. 6: Numerical results for physically motivated ferromagnetic model, left: magnetization, right: magnetostriction vs. magnetic field

In Fig. 6 results from the microphysical model are shown in terms of magnetization and magnetostriction. As intended, a hysteresis behavior is obtained, although the area of the loops is smaller than for ferroelectric materials. Further, as in Fig. 2 a saturation is observed for large magnetic fields. In Fig. 7, results are presented for the phenomenological model based on the simple approach with constant values $\zeta_1 = \zeta_1^0$, $\zeta_2 = \zeta_2^0$ and $\xi = \xi^0$. As expected, the curves are nonlinear but reversible. They agree qualitatively with those in Fig. 3. The fact that cobalt ferrite has been used to demonstrate both hysteresis and reversible behaviours is based on experimental observations, where this material proved to be able to exhibit both kinds of features, depending on the manufacturing conditions [14].

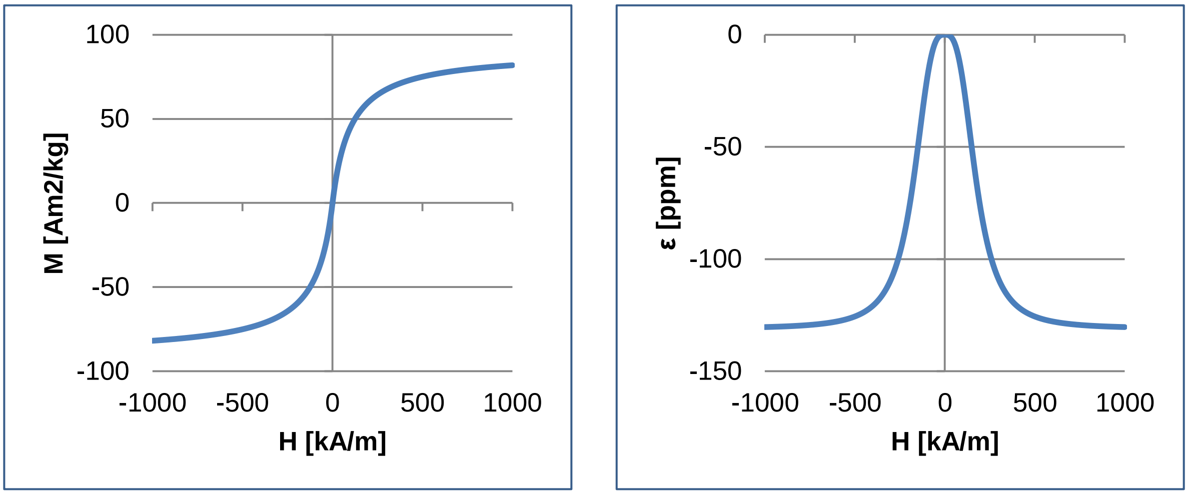

Fig. 7: Numerical results for phenomenological ferromagnetic model, left: magnetization, right: magnetostriction vs. magnetic field

In Fig. 8, the effect of a superimposed mechanical load on the magnetostrictive properties in terms of the strain-magnetic field curve is investigated, based on the phenomenological model. In contrast to Fig. 7, the more sophisticated model has been used, where ζ_1, ζ_2 and ξ depend on the stresses according to Eq. (22). The blue plots represent a pure magnetic loading in x_1-direction, whereas the red plots stand for the combined loading. The solid lines show the strain in the direction of the magnetic field, the dashed lines in the perpendicular direction. The plots are in agreement to what is expected intuitively. The tensile stress in x_2-direction supports the magnetic field and leads to a saturation at lower magnetic loads. Further, the absolute value of the strain is larger in the direction of the magnetic field than perpendicular to it.

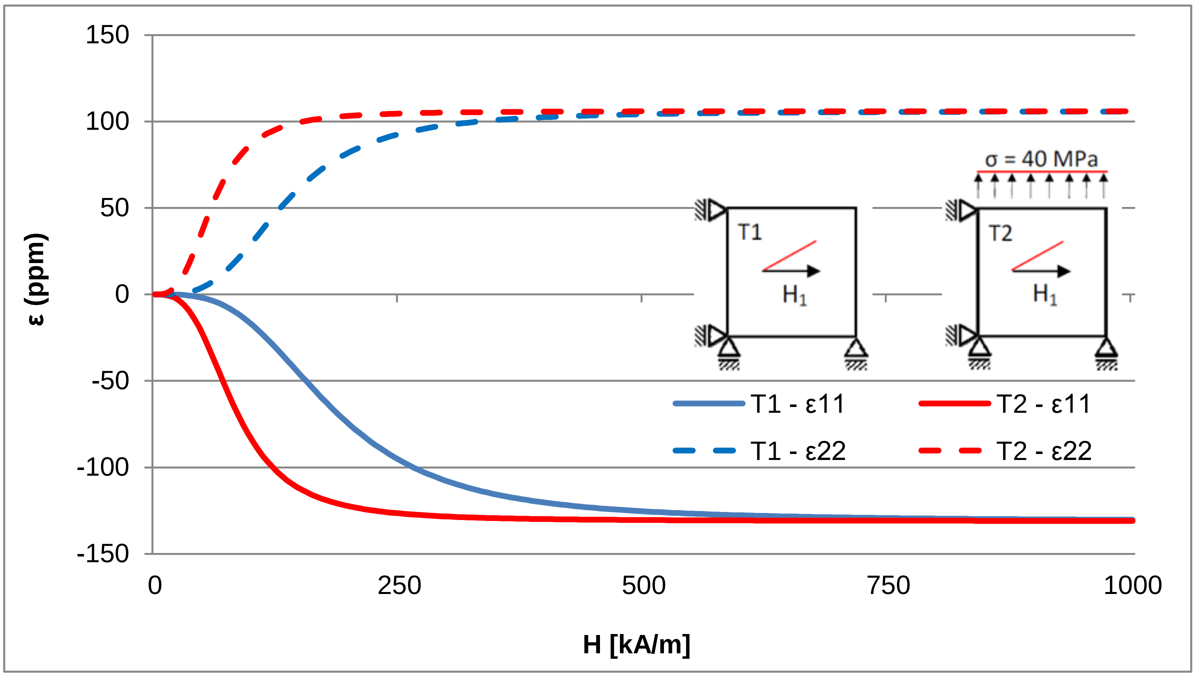

Fig. 8: Numerical results for phenomenological ferromagnetic model at combined magnetomechanical loading

5 CONCLUSIONS

Two types of constitutive models for ferroelectric materials have been presented. The one is based on physical considerations on the micro- and meso-levels, the other is purely phenomenological. The one produces irreversible hysteresis behavior and the other exhibits non-linear reversible features. Both characteristics are well-known from different ferromagnetic materials. Due to possible applications of the models with respect to multiferroic composites, dielectric properties are included in both constitutive approaches. The material models have been implemented within a finite element context to be able to investigate complex boundary value problems. Verifications of the constitutive models demonstrate their capability of describing ferroelectric material behavior appropriately.

REFERENCES

[1] Scott, J. F.: *Data storage: Multiferroic memories*. Nat Mater **6** (4), 256–257, 2007.

[2] Fiebig, M.: *Revival of the magnetoelectric effect*. J. of Phys. D: App. Phys. **38** (8), R123 – R152, 2005.

[3] Nan, C.-W.: *Magnetoelectric effect in composites of piezoelectric and piezomagnetic phases*. Phys. Rev. B **50** (9), 6082–6088, 1994.

[4] Buchanan, G. R.: *Layered versus multiphase magneto-electro-elastic composites*. Compos Part B: Eng. **35** (5), 413–420, 2004.

[5] Aboudi, J.: *Micromechanical analysis of fully coupled electro-magneto-thermo-elastic multiphase composites*. Smart Mater. Struct. **10** (5), 867–877, 2001.

[6] Lu, X. Y., Li, H., Wang, B.: *Theoretical analysis of electric, magnetic and magnetoelectric properties of nano-structured multiferroic composites*. J. Mech. Phys. Sol. **59** (10), 1966–1977, 2011.

[7] Linnemann, K., Klinkel, S., Wagner, W.: *A constitutive model for magnetostrictive and piezoelectric materials*. Int. J. Solids Struct. **46**, 1149-1166, 2009.

[8] Bozorth, R.: *Ferromagnetism*. Van Nostrand, New York, 1951.

[9] Stefanita, C.-G.: *Magnetism. Basics and applications*. Springer, Heidelberg / New York, 2012.

[10] Bergmann, L., Schaefer, C.: *Lehrbuch der Experimentalphysik*. 6: Festkorper. de Gruyter, Berlin / New York, 2005.

[11] Du Trémolet de Lacheisserie, E., Gignoux, D., Schlenker, M.: *Magnetism. Materials and applications*. Springer, New York, 2005.

[12] Kittel, C.: *Einführung in die Festkörperphysik*. 14. Oldenbourg, München, 2006.

[13] Morrish, A. H.: *The physical principles of magnetism*. IEEE Press, New York, 2001.

[14] Mohaideen, K. K., Joy, P. A.: *Studies on the effect of sintering conditions on the magnetostriction characteristics of cobalt ferrite derived from nanocrystalline powders*. J. European Ceramic Society **34** (3), 677–686, 2014.

[15] Avakian, A., Gellmann, R., Ricoeur, A.: *Nonlinear modeling and finite element simulation of magnetoelectric coupling and residual stress in multiferroic composites*. Acta Mechanica (2015), DOI: 10.1007/s00707-015-1336-0

[16] Lange, S., Ricoeur, A.: *A condensed microelectromechanical approach for modeling tetragonal ferroelectrics*. Int. J. Solids Struct. **54**, 100–110, 2015.

[17] Kellogg, R. A., Flatau, A., Clark, A. E., Wun-Fogle, M., Lograsso, T.: *Quasi-static Transduction Characterization of Galfenol*. J. *Intell. Mat. Syst. Struct.* **16** (6), 471–479, 2005.

[18] Chen, P. J., Tucker, T. J.: *Determination of the polar equilibrium properties of the ferroelectric ceramic PZT 65/35*. Acta Mechanica **38** (3-4), 209–218, 1981.

[19] Hwang, S. C., Lynch, C. S., McMeeking, R. M.: *Ferroelectric/ferroelastic interactions and a polarization switching model*. Acta metall. mater. **43** (5), 2073–2084, 1995.

[20] Kessler, H., Balke, H.: *On the local and average energy release in polarization switching phenomena*. J. Mech. Phys. Sol. **49** (5), 953–978, 2001.

[21] Kamlah, M., Liskowsky, A. C., McMeeking, R. M., Balke, H.: *Finite element simulation of a polycristalline ferroelectric based on a multidomain single crystal switching model*. Int. J. Solids Struct. **42** (9-10), 2949–2964, 2005.

[22] Tang, T. and Yu, W.: *Micromechanical modeling of the multiphysical behavior of smart materials using the variational asymptotic method*. Smart Mater. Struct **18** (12), 125026, 2009.

[23] Zheng, Y. X., Cao, Q. Q., Zhang, C. L., Xuan, H. C., Wang, L. Y., Wang, D. H., Du, Y. W.: *Study of uniaxial magnetism and enhanced magnetostriction in magnetic-annealed polycrystalline CoFe2O4*. *J. Appl. Phys.* **110** (4), 043908, 2011.